Gas–Liquid Mass-Transfer Properties in CO_2 Absorption System with Ionic Liquids

Xin Zhang, Di Bao, Ying Huang, Haifeng Dong, Xiangping Zhang, and Suojiang Zhang
Beijing Key Laboratory of Ionic Liquids Clean Process, State Key Laboratory of Multiphase Complex Systems, Key Laboratory of Green Process and Engineering, Institute of Process Engineering, Chinese Academy of Sciences, Beijing 100190, P.R. China

College of Chemistry and Chemical Engineering, University of Chinese Academy of Sciences, Beijing 100049, P.R. China

DOI 10.1002/aic.14507
Published online June 3, 2014 in Wiley Online Library (wileyonlinelibrary.com)

The deficiency of mass-transfer properties in ionic liquids (ILs) has become a bottleneck in developing the novel IL-based CO_2 capture processes. In this study, the liquid-side mass-transfer coefficients (k_L) were measured systematically in a stirred cell reactor by the decreasing pressure method at temperatures ranging from 303 to 323 K and over a wide range of IL concentrations from 0 to 100 wt %. Based on the data of k_L, the kinetics of chemical absorption of CO_2 with mixed solvents containing 30 wt % monoethanolamine (MEA) and 0–70 wt % ILs were investigated. The k_L in IL systems is influenced not only by the viscosity but also the molecular structures of ILs. The enhancement factors and the reaction activation energy were quantified. Considering both the mass-transfer rates and the stability of IL in CO_2 absorption system, the new IL-based system MEA + [bmim][NO_3] + H_2O is recommended. © 2014 American Institute of Chemical Engineers *AIChE J*, 60: 2929–2939, 2014

Keywords: ionic liquids, carbon dioxide, mass-transfer coefficient, kinetics, absorption

Introduction

Carbon dioxide (CO_2) emission from burning fossil fuels is considered as a main contributor for global warming and climate change. Therefore, the removal of CO_2 from gas streams has been a hot spot, and many researchers are developing and improving efficient technologies for CO_2 absorption. For gas streams with a high CO_2 composition, physical absorption using physical solvent such as methanol, sulfolane, and propylene carbonate is recommended. Alkanolamines including primary, secondary, tertiary, and hindered amines are the widely used chemical solvents which can enhance CO_2 absorption rate and capacity.[1–4] Among the alkanolamines, aqueous monoethanolamine (MEA) is the most used absorbent due to its high reaction rate, high absorption capacity on a weight basis, high thermal stability, and low cost. However, the MEA process has several drawbacks such as degradation of amine, corrosion, high energy consumption during regeneration, and the loss of the amine into gas stream.

Ionic liquids (ILs), entirely composed of ions, have been paid much attention and are regarded as attractive solvents for CO_2 capture considering their unique characteristics like negligible vapor pressure, tunable physicochemical properties and relatively high CO_2 solubility.[5–7] Brennecke's research group[8] first reported that CO_2 showed excellent solubility in IL [bmim][PF_6] in 1999, reaching a 0.72 mole fraction at 313 K and 9.3 MPa. Zhang's research group[9] measured the solubilities of CO_2 in a series of conventional imidazolium-based tetrafluoroborate ILs. However, the absorption performance of conventional ILs still cannot compete with the present technology due to the lower CO_2 absorption capacity. Incorporating functional groups to the anion or cation of ILs to form task-specific ionic liquids (TSILs), such as cation-functionalized ILs,[10] anion-functionalized ILs,[11,12] dual amino-functionalized ILs,[13,14] is another way to enhance the CO_2 absorption capacity. Although TSILs with amino groups can dramatically increase the CO_2 absorption ability, the synthetic procedures and the purification steps are usually complex. Therefore, TSILs coupled with high viscosities and relatively high production costs are also not cost-competitive with conventional absorbent like MEA. A new strategy to make ILs being directly applied in the carbon capture system is to blend ILs with amines. These mixtures retain the desired properties of ILs for CO_2 capture but avoid some inherent drawbacks such as high viscosity, intractable tars, and high cost.[15–17] Replacing certain amount of water with ILs can reduce the energy consumption in the solvent regeneration process and decrease the loss of amine into the gas stream.[15,18,19]

In a gas–liquid mass-transfer system, studying the k_L will provide important engineering basic data, which is essential for suitable design and operation of industrial units. The mass-transfer characteristics in the stirred tank operating with conventional solvents such as water,[20–22] glucose,[23] and glycerol[23] have been investigated widely by measuring the

Correspondence concerning this article should be addressed to X. Zhang at xpzhang@home.ipe.ac.cn (or) S. Zhang at sjzhang@home.ipe.ac.cn.

k_L with experiments in the literature. As for the aspect of ILs, the studies are scant. In our previous works,[24–28] the CO_2 bubble behaviors in IL systems have been investigated experimentally and numerically in a bubble column, which provided basic transport and fluid dynamics knowledge for carbon capture system with ILs. The mass-transfer characteristics of CO_2 absorption have also been investigated in a rotating packed bed contactor using pure IL [bmim][PF_6].[29] Sánchez et al.[30] studied the kinetics of the reaction of CO_2 with amino-functionalized IL [apmim][BF_4] at 303 and 333 K. Ahmady et al.[31] and Lu et al.[32] reported the kinetics of CO_2 absorption by the blends of *N*-methyldiethanolamine (MDEA) or MEA with IL [bmim][BF_4]. However, those ILs, which were selected in the literature, are unstable and harmful to the environment because of producing the toxic gas HF.[33] The aim of this work is to study the mass-transfer properties on the promising IL-based carbon capture system, which we believe have great potential for large-scale applications.

This study mainly focuses on two respects. In one respect, the liquid-side mass-transfer coefficient of CO_2 in IL-H_2O systems was determined from the fall in pressure, and effects of several parameters (i.e., different ILs, absorption temperature, stirrer speed, and IL concentration) on the k_L were evaluated and analyzed. In another respect, based on the data of k_L, the kinetics of the reaction between CO_2 and different MEA-IL-H_2O systems were studied. The influence of IL concentration on kinetic parameters was interpreted. The enhancement factors owing to the chemical reaction were quantified. The reaction activation energy of CO_2 chemical absorption into MEA- [bmim][NO_3]-H_2O system has been quantified.

Theory

Liquid-side mass-transfer coefficient determination

The mass-transfer coefficient in the liquid phase, which is necessary for calculating the reaction rate constant, was obtained from experimental data of CO_2 absorption in IL-H_2O systems by the pressure drop method. The overall mass-transfer flux (N) in the physical absorption process can be interpreted by Eq. 1, which is the dynamic mass balance over the gas phase

$$N_{CO_2}=\frac{V_G}{ZRT}\left(-\frac{dP_{CO_2}}{dt}\right)=k_L A\left(\frac{P_{CO_2}}{K_H}-C_{CO_2}\right) \tag{1}$$

where C_{CO_2} is the absorbed gas concentration in the liquid bulk, A is the gas–liquid interfacial area, Z is the compressibility factor, K_H is Henry's constant, and V_G is the volume of gas above the liquid in the stirred reactor. Considering the mass balance of CO_2 in the stirred reactor, where CO_2 leaving the gas enters the liquid, C_{CO_2} is obtained from

$$C_{CO_2}=\frac{(P^0_{CO_2}-P_{CO_2})V_G}{ZRTV_L} \tag{2}$$

Then the partial pressure of CO_2 is obtained as follows

$$P^0_{CO_2}=P^0-P_{Vapor} \tag{3}$$

where P^0 is the initial total pressure and P_{Vapor} is the vapor pressure of the solvent before CO_2 loading. P_{CO_2} i.s also obtained by subtracting the vapor pressure of the solvent. After the integration of Eq. 1, the liquid-side mass-transfer coefficient is obtained

$$k_L at=\frac{\beta}{1+\beta}\ln\left[\frac{P^0_{CO_2}}{(1+\beta)P_{CO_2}-\beta P^0_{CO_2}}\right] \tag{4}$$

where $a=A/V_L$ and the parameter β is given by

$$\beta=\frac{V_G K_H}{ZRTV_L} \tag{5}$$

Equation 4 indicates that once the right-hand side of Eq. 4 is obtained, the volumetric mass-transfer coefficient within the time interval [0, t] can be determined by the linear fitting method.

CO_2 absorption kinetics

Reaction Mechanism. The zwitterion mechanism proposed by Caplow[34] and later reintroduced by Danckwerts[35] is generally accepted as the reaction mechanism between CO_2 and MEA, which involves the formation of a "zwitterion"

$$CO_2+MEA \underset{k_{-1}}{\overset{k_1}{\rightleftarrows}} MEAH^+COO^- \tag{6}$$

and the subsequent deprotonation of the zwitterion by a base B

$$MEAH^+COO^-+B\xrightarrow{k_B}MEACOO^-+BH^+ \tag{7}$$

The base B can be MEA, OH^-, H_2O, CO_3^{2-}, andHCO_3^- in the MEA-IL-H_2O system, because there is no chemical reaction between CO_2 with conventional IL like [bmim][BF_4].[31] The reaction of CO_2 with MEA can be deduced from Eqs. 6 and 7 by adopting the steady-state principle to the zwitterion

$$r_{CO_2}=\frac{k_1 C_{MEA} C_{CO_2}}{1+\frac{k_{-1}}{\sum k_B C_B}} \tag{8}$$

In comparison with the reverse reaction in Eq. 6, the deprotonation process from the zwitterion is almost instantaneous and the rate determining procedure is the zwitterion formation process,[2] namely

$$k_{-1}\ll\sum k_B C_B \tag{9}$$

hence, Eq. 8 can be rewritten into the form

$$r_{CO_2}=k_1 C_{MEA} C_{CO_2} \tag{10}$$

Kinetic Parameters Determination. The enhancement factor E over physical absorption is usually introduced to reflect the influence of chemical reaction on the absorption kinetics. Since the excess MEA was added to the reactor, it is safe to assume that the CO_2 concentration in the liquid bulk is 0. Therefore, the overall mass-transfer flux in the chemical absorption process can be calculated by Eq. 11

$$N_{CO_2}=\frac{V_G}{ZRT}\left(-\frac{dP_{CO_2}}{dt}\right)=Ek_L A\frac{P_{CO_2}}{K_H} \tag{11}$$

after integration

$$\ln P_{CO_2}=\ln P^0_{CO_2}-\frac{Ek_L a}{\beta}t \tag{12}$$

The enhancement factor is also obtained by the graphic method, namely calculating the slope of the left-hand side of

Table 1. Criterions for Different Reaction Regimes

Reaction Regime	Criterion	Description
Instantaneous	$Ha >> 3$	$E = E_\infty$
Fast	$Ha > 3$	$E = Ha$
Intermediate	$0.3 < Ha < 3$	$E = Ha/\tan h(Ha)$
Slow	$Ha < 0.3$	$E = 1$

Eq. 12 vs. time. For each experiment of CO_2 chemical absorption into the MEA-IL-H_2O system, the conditions were maintained to ensure that the absorption occurred in the pseudofirst-order reaction regime which requires

$$E_\infty \gg Ha > 3 \tag{13}$$

where the Hatta number is

$$Ha = \frac{\sqrt{k_2 C_{\mathrm{MEA}} D_{\mathrm{CO_2}}}}{k_{\mathrm{L}}} \tag{14}$$

and E_∞ is the infinite enhancement factor, defined as

$$E_\infty = 1 + \frac{D_{\mathrm{MEA}} C_{\mathrm{MEA}}}{v D_{\mathrm{CO_2}} C_{\mathrm{CO_2}}} \tag{15}$$

where v is the stoichiometric coefficient, D_{MEA} and $D_{\mathrm{CO_2}}$ are the diffusivities of MEA and CO_2 in the liquid, respectively. The criterions for different reaction regimes were presented in Table 1. When the Eq. 13 is satisfied, the reaction is in the fast reaction regime and the enhancement factor E is equal to Ha. Then the second-order reaction rate constant k_2 can be calculated using Eqs. 12 and 14

$$k_2 = \frac{(E k_{\mathrm{L}})^2}{C_{MEA} D_{\mathrm{CO_2}}} \tag{16}$$

Experimental Section

Materials preparation

CO_2 gas was supplied by Beiwen Gas Co. with a purity $\geq 99.99\%$ and was used without further purification. MEA (99.5%) was provided by Beijing Chemical Works. Four different kinds of ILs ([bmim][BF_4], [bmim][NO_3], [bmim][$N(CN)_2$], and [omim][BF_4]) with a purity of 99.0% were purchased from Linzhou Keneng Technology Co. The ILs were dried under vacuum for 48 h 333 K and then kept in a drying cabinet before used. The water contents of the ILs after drying were confirmed to be < 200 ppm by Karl-Fisher titration. Deionized water was boiled to remove the dissolved gases before utilization.

Table 2. Dimensions of the Experimental Apparatus

Parameters	Value	Unit
Inner Diameter of Reactor	4	cm
Height of Reactor	8	cm
Total Volume of Reactor + Gas Pipeline	105	mL
Volume of Liquid	~20	mL
Volume of Gas Reservoir	500	mL
Interfacial Area	12.56	cm^2
Stirrer Speed	100–250	Rpm

Experimental apparatus and procedure

Figure 1 presents the schematic diagram of the experimental apparatus. It mainly consists of a 316-L stainless steel reactor with a magnetic stirrer, a gas reservoir, a vacuum pump, a water bath, and two pressure sensors (Rosemount 3051) with an accuracy of 0.15 kPa in the experimental pressure range. The gas reservoir is applied in the present study in order to preheat the CO_2 and control the CO_2 flow rates into the reactor. Both the stirred cell reactor and the gas reservoir allow a maximum pressure of 10 MPa. The temperature in the reactor is maintained with an uncertainty of ± 0.1 K using an external water bath which is connected to the jackets of the reactor and the gas reservoir. Detailed information about the equipment is presented in Table 2. Before conducting the experiments, pure water with the similar volume of the absorbent was added to the reactor due to its low viscosity. The specific stirrer speed range was selected to ensure the smooth gas–liquid interface by observation. Since the viscosities of the different absorbents used in this study are all greater than that of water. Therefore, the undisturbed gas–liquid interface was created during the experiments.

A series of experiments were conducted to study the mass-transfer characteristics. For each experimental run, about 20 mL freshly prepared absorbent was placed in the reactor. The reactor was closed and kept under vacuum (2 kPa) at the operating temperatures to degas the absorbent as well as to test the gas leak. This procedure lasted for 1 h to ensure that the temperature equilibrium had been reached. After that, the vapor pressure of the absorbent was recorded. Then a certain amount of CO_2 was introduced to the gas

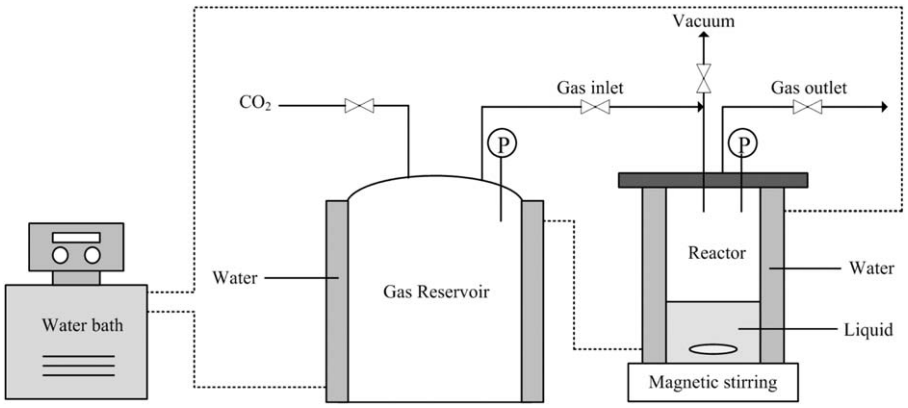

Figure 1. Schematic diagram of the experimental apparatus.

Table 3. Densities and Viscosities of IL-H_2O Systems

	Composition of the Absorbent					Composition of the Absorbent			
T (K)	IL	H_2O	ρ_l(g·cm^{-3})	μ_l(mPa s)	T (K)	IL	H_2O (wt %)	ρ_l (g·cm^{-3})	μ_l (mPa s)
313	[bmim][$N(CN)_2$]	< 200ppm	1.051521	18.1576	303	95 wt %[bmim][NO_3]	5	1.14786	35.7366
313	[bmim][BF_4]	< 200ppm	1.191293	56.3556	308	95 wt %[bmim][NO_3]	5	1.144616	29.4877
313	[bmim][NO_3]	< 200ppm	1.153284	89.9147	313	95 wt %[bmim][NO_3]	5	1.141377	24.6353
313	[omim][BF_4]	< 200ppm	1.093232	135.9992	318	95 wt %[bmim][NO_3]	5	1.138161	20.8564
303	95 wt% [bmim][BF_4]	5 wt%	1.181645	18.8686	323	95 wt%[bmim][NO_3]	5	1.134947	17.8828
308	95 wt% [bmim][BF_4]	5 wt%	1.178004	16.0355	303	90 wt%[bmim][NO_3]	10	1.134676	17.209
313	95 wt% [bmim][BF_4]	5 wt%	1.17438	13.8683	308	90 wt%[bmim][NO_3]	10	1.131348	14.6742
318	95 wt% [bmim][BF_4]	5 wt%	1.170772	12.1043	313	90 wt%[bmim][NO_3]	10	1.128034	12.645
323	95 wt% [bmim][BF_4]	5 wt%	1.167171	10.665	318	90 wt%[bmim][NO_3]	10	1.12472	11.001
303	95 wt% [omim][BF_4]	5 wt%	1.090741	42.6659	323	90 wt%[bmim][NO_3]	10	1.121408	9.6607
308	95 wt% [omim][BF_4]	5 wt%	1.086471	34.9096	313	80 wt%[bmim][NO_3]	20	1.118244	6.3143
313	95 wt% [omim][BF_4]	5 wt%	1.0822	28.9041	313	70 wt%[bmim][NO_3]	30	1.100881	3.9077
318	95 wt% [omim][BF_4]	5 wt%	1.077929	24.2954	313	60 wt%[bmim][NO_3]	40	1.083209	2.7534
323	95 wt% [omim][BF_4]	5 wt%	1.073658	20.6284	313	50 wt%[bmim][NO_3]	50	1.066967	2.1958
303	95 wt% [bmim][$N(CN)_2$]	5 wt%	1.053407	15.0254	313	40 wt%[bmim][NO_3]	60	1.050311	1.464
308	95 wt% [bmim][$N(CN)_2$]	5 wt%	1.050177	12.9385	313	30 wt%[bmim][NO_3]	70	1.035238	1.2402
313	95 wt% [bmim][$N(CN)_2$]	5 wt%	1.046963	11.2712	313	20 wt%[bmim][NO_3]	80	1.019862	0.9709
318	95 wt% [bmim][$N(CN)_2$]	5 wt%	1.043773	9.905	313	10 wt%[bmim][NO_3]	90	1.005944	0.8194
323	95 wt% [bmim][$N(CN)_2$]	5 wt%	1.040592	8.7735					

reservoir supplied by the gas cylinder. The inlet gas valve was open until the pressure reached the desired value and the agitation was turned on. The fall in pressure was recorded for the first 10 min of the experiments using a data acquisition system. The equilibrium pressure was considered to have been reached when the pressure changed less than 1 kPa for a period of 1 h. All experiments were repeated at least three times to guarantee the reproducibility of the results.

Physical Properties

Density and viscosity

The densities of different IL systems were measured by a density meter (Anton Paar DMA 5000, Anton Paar Co., Austria) with the accuracy of ± 0.000005 g·cm^{-3} at temperatures ranging from 303 to 323 K. The viscosities were determined by an Automated Microviscometer (Anton Paar AMVn, Anton Paar Co., Austria) with a reproducibility <0.5% and a repeatability <0.1%. The detailed density and viscosity data of IL-H_2O systems and MEA-IL-H_2O systems are available in Tables 3 and 4, respectively.

Diffusivity

The diffusivities of CO_2 in the MEA-IL-H_2O systems were determined by N_2O analogy which presented the following relation

$$\frac{D_{CO_2}}{D_{N_2O}} = \frac{D_{CO_2,w}}{D_{N_2O,w}} \tag{17}$$

Versteeg and van Swaaij[36] proposed the following expressions to calculate the diffusivities of N_2O and CO_2 in water

$$D_{CO_2,w} = 2.35 \times 10^{-6} e^{-2119/T} \tag{18}$$

$$D_{N_2O,w} = 5.07 \times 10^{-6} e^{-2371/T} \tag{19}$$

The diffusivity of N_2O into MEA-IL-H_2O systems was estimated by Eq. 20.

$$\frac{D_{N_2O,w}}{D_{N_2O}} = \left(\frac{\mu}{\mu_w}\right)^{\gamma} \tag{20}$$

where μ and μ_w are the viscosities of the MEA-IL-H_2O solution and the water, respectively. According to the recommendation by Sada et al.,[37] the value of γ is 0.51 for MEA solutions.

The commonly applied empirical correlation Wilke-Chang equation[38] was used to calculate the diffusivity of MEA in MEA-IL-H_2O systems

$$D_{MEA} = \frac{7.4 \times 10^{-8} \sqrt{\varphi M_{IL\text{-}H_2O}}\, T}{\mu_{IL\text{-}H_2O} V_{MEA}^{0.6}} \tag{21}$$

where $M_{IL\text{-}H_2O}$ is the mean molecular weight of IL-H_2O solutions, T is temperature, $\mu_{IL\text{-}H_2O}$ is the viscosity of the IL-H_2O solutions, V_{MEA} is molar volume of MEA at its normal boiling point and φ is the solvent association factor with a value of 2.6.

Results and Discussion

CO_2 solubility in IL systems

The CO_2 solubility is an essential parameter to calculate the Henry's constant, and the Henry's constant, as Eq. 4 shows, is necessary for evaluating the liquid-side mass-transfer coefficient in IL systems. The mole fractions of absorbed CO_2 into the IL systems, x_{CO_2}, are calculated using the following equations

$$n_{CO_2} = \frac{(P^0_{CO_2} - P_{Vapor})V_G}{Z_1 RT} - \frac{(P^e_{CO_2} - P_{Vapor})V_G}{Z_2 RT} \tag{22}$$

$$x_{CO_2} = \frac{n_{CO_2}}{n_{CO_2} + n_{IL} + n_{H_2O}} \tag{23}$$

where Z_1 and Z_2 are the compressibility factors corresponding to the initial and equilibrium pressure in the reactor.

To test the applicability of the present experimental setup, the solubility of CO_2 in [bmim][BF_4] and [bmim][NO_3] at 313 K were measured and compared with the data reported by Brennecke's research group.[39] Figure 2 shows that the

Table 4. Densities and Viscosities ofMEA-IL-H_2O Systems

Composition of the Absorbent						Composition of the Absorbent					
T (K)	IL	H_2O (wt %)	MEA (wt %)	ρ_l (g·cm^{-3})	μ_l (mPa s)	T (K)	IL	H_2O (wt %)	MEA (wt %)	ρ_l (g·cm^{-3})	μ_l (mPa s)
303	65 wt% [bmim][BF_4]	5	30	1.12344	16.8857	323	65 wt% [bmim][NO_3]	5	30	1.086125	9.1984
308	65 wt% [bmim][BF_4]	5	30	1.119521	13.8146	303	60 wt% [bmim][NO_3]	10	30	1.099964	15.0702
313	65 wt% [bmim][BF_4]	5	30	1.115614	11.5129	308	60 wt% [bmim][NO_3]	10	30	1.096386	12.5408
318	65 wt% [bmim][BF_4]	5	30	1.111722	9.7792	313	60 wt% [bmim][NO_3]	10	30	1.092818	10.5835
323	65 wt% [bmim][BF_4]	5	30	1.107814	8.3422	318	60 wt% [bmim][NO_3]	10	30	1.089262	9.0515
303	65 wt% [bmim][$N(CN)_2$]	5	30	1.037781	11.7301	323	60 wt% [bmim][NO_3]	10	30	1.085702	7.8079
308	65 wt% [bmim][$N(CN)_2$]	5	30	1.034288	9.987	313	70 wt% [bmim][NO_3]	0	30	1.100226	17.7662
313	65 wt% [bmim][$N(CN)_2$]	5	30	1.090801	8.5885	313	50 wt% [bmim][NO_3]	20	30	1.076913	6.8974
318	65 wt% [bmim][$N(CN)_2$]	5	30	1.027323	7.4589	313	40 wt% [bmim][NO_3]	30	30	1.063372	4.9402
323	65 wt% [bmim][$N(CN)_2$]	5	30	1.023846	6.5283	313	30 wt% [bmim][NO_3]	40	30	1.048568	3.7014
303	65 wt% [bmim][NO_3]	5	30	1.100548	17.9784	313	20 wt% [bmim][NO_3]	50	30	1.033771	2.9002
308	65 wt% [bmim][NO_3]	5	30	1.096951	14.9258	313	10 wt% [bmim][NO_3]	60	30	1.018496	2.3417
313	65 wt% [bmim][NO_3]	5	30	1.093341	12.5531	313	0	70	30	1.003422	1.9631
318	65 wt% [bmim][NO_3]	5	30	1.089731	10.6855						

results are in good agreement with the literature,[39] confirming the accuracy of CO_2 solubility in the present experimental setup. The CO_2 solubility in different IL systems has been illustrated in Figure 3. It shows that [bmim][BF_4] presents a greater capability of absorbing CO_2 compared with [bmim][NO_3] when adding the same amount of water (5 wt %) to the IL. Regarding the effect of water content on the CO_2 solubility, it presents that the CO_2 solubility decreases with the increasing water content from 5 to 10 wt % in IL. Furthermore, the equilibrium pressure is approximately described as a linearly increasing function of the mole fraction, which facilitates the calculation of Henry's constant discussed in the next part.

Henry's law constant

The Henry's law constant can be calculated according to the literature[40]

$$H=\lim_{x_{CO_2}\to 0}\frac{f(P^e_{CO_2},T)}{x_{CO_2}}\cong\frac{\phi_{CO_2}P^e_{CO_2}}{x_{CO_2}} \tag{24}$$

where H is the Henry's law constant, f is the fugacity at the equilibrium temperature, and equilibrium pressure, ϕ_{CO_2} is the fugacity coefficient which can be calculated by the RK EOS[41]

$$P=\frac{RT}{V-b}-\frac{a}{T^{0.5}V(V+b)} \tag{25}$$

$$\ln\phi_{CO_2}=Z-1-\ln(Z-BP)-\frac{A^2}{B}\ln\left(1+\frac{BP}{Z}\right) \tag{26}$$

where

$$a=\frac{0.42748R^2T_C^{2.5}}{P_C} \tag{27}$$

$$b=\frac{0.08664RT_C}{P_C} \tag{28}$$

and

$$A^2=\frac{a}{R^2T^{2.5}} \tag{29}$$

$$B=\frac{b}{RT} \tag{30}$$

where a, b, A^2, and B are the parameters of RK EOS, V is the molar volume and T_c, P_c are the critical temperature and the critical pressure of CO_2, respectively.

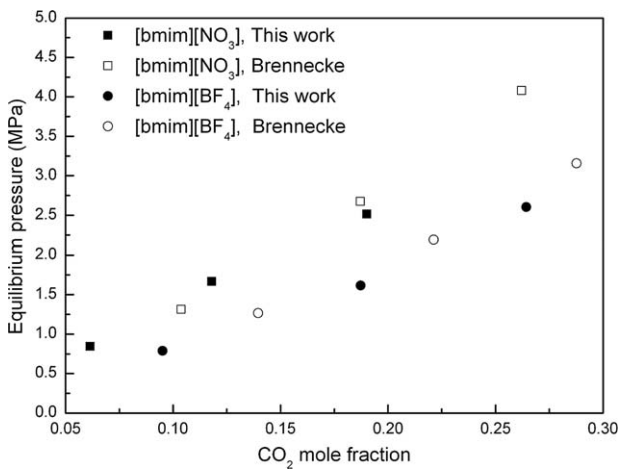

Figure 2. The solubility of CO_2 in ILs ■, • this work; □, ○ Brennecke's research group.[39]

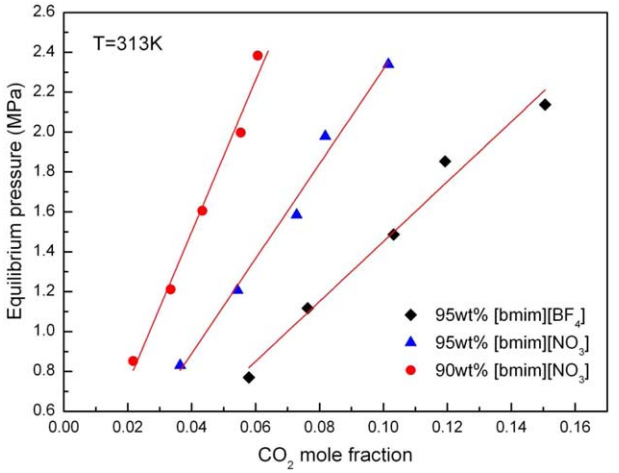

Figure 3. The solubility of CO_2 in different IL-H2O systems.

[Color figure can be viewed in the online issue, which is available at wileyonlinelibrary.com.]

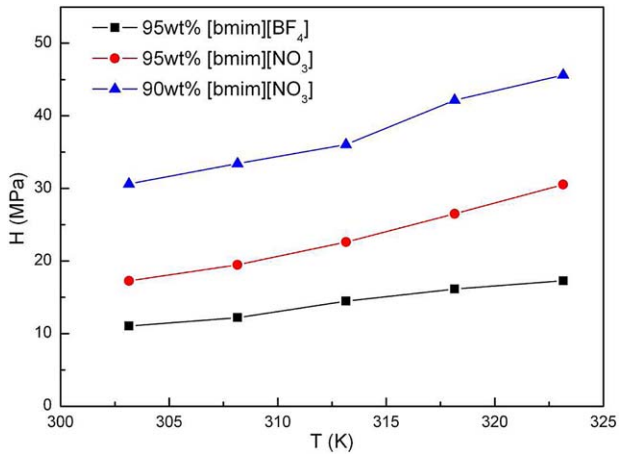

Figure 4. Effect of temperatureon Henry's constant in different IL-H_2O systems.

[Color figure can be viewed in the online issue, which is available at wileyonlinelibrary.com.]

As shown in Figure 4, the Henry's constant increases, namely the CO_2 solubility decreases with the increase of temperature in IL-H_2O systems. Figure 4 also shows that the order of Henry's constant in different IL systems is 90 wt % [bmim][NO_3] > 95 wt % [bmim][NO_3] > 95 wt % [bmim][BF_4], which is in accordance with the previous discussion about the CO_2 solubility.

Liquid-side mass-transfer coefficient

Effect of IL Structure. The liquid-side mass-transfer coefficient was calculated by Eq. 4 based on the pressure drop in the reactor. Four different kinds of pure ILs ([bmim][BF_4], [omim][BF_4], [bmim][NO_3], and [bmim][$N(CN)_2$]) were selected due to their similar structures (same anion or same cation). Both the anions and cations of ILs have great impact on the CO_2 solubility in ILs.[42] The Henry's constants of CO_2 absorption in [omim][BF_4], [bmim][BF_4], 95 wt % [bmim][BF_4] and pure water at 313 K were measured, indicating a value of 6.52, 8.15, 14.46, and 236 MPa, respectively. Therefore, the CO_2 solubility is much higher in ILs and IL-H_2O mixtures than that of in water. It also shows that the CO_2 solubility increases with increasing the length of the alkyl side chain on the imidazolium ring

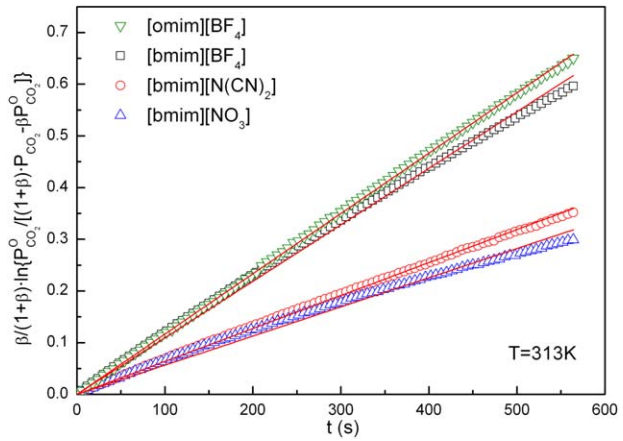

Figure 5. k_La determination in different ILs.

[Color figure can be viewed in the online issue, which is available at wileyonlinelibrary.com.]

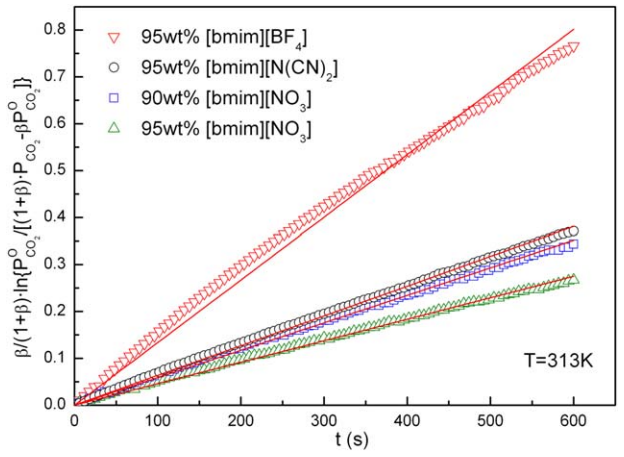

Figure 6. k_La determinationin different IL-H_2O systems.

[Color figure can be viewed in the online issue, which is available at wileyonlinelibrary.com.]

([bmim]$^+$ < [omim]$^+$) when they have same anion. For the ILs with same cation, the CO_2 solubility increases in the order of $[NO_3]^- < [N(CN)_2]^- < [BF_4]^-$. A typical plot for k_L determination in pure ILs at 313 K has been presented in Figure 5. It displays that the right-hand side of Eq. 4 can be depicted as a good linear function of time in all cases, which verifies the reliability of the method for calculating k_L used in this work. Figure 5 also shows that the slopes are ranked as [bmim][NO_3] < [bmim][$N(CN)_2$] < [bmim][BF_4] < [omim][BF_4], indicating that the maximum k_L exists in [omim][BF_4] while the minimum is in [bmim][NO_3]. However, the order of k_L is not consistent with the order of the viscosities of ILs which have been presented in Table 3. According to the traditional ideas, the k_L mainly depends on the diffusivity of CO_2 in the liquid. In other words, the k_L is influenced by the viscosity. Therefore, the k_L in [bmim][$N(CN)_2$] should be greater than that in [bmim][BF_4] when only the effect of viscosity is taken into consideration. As described previously about the anionic structure of ILs, the CO_2 solubility in [bmim][$N(CN)_2$] is lower than that in [bmim][BF_4] which shows the same tendency as k_L. From the viewpoint of molecular dynamics, CO_2 is located in the interstices formed by the strong Coulombic interactions between cations and

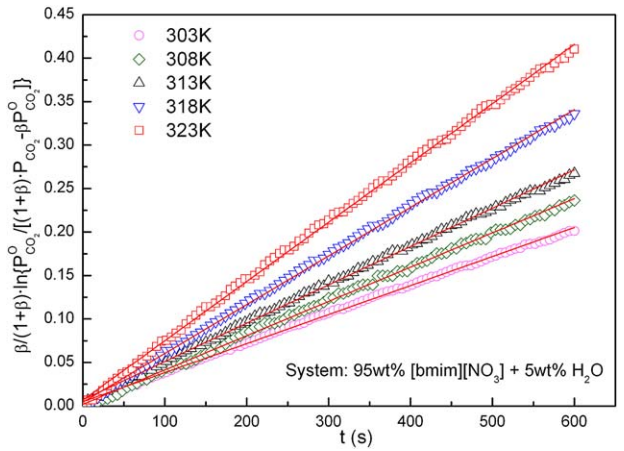

Figure 7. Effect of temperature on k_La determination in IL-H_2O system.

[Color figure can be viewed in the online issue, which is available at wileyonlinelibrary.com.]

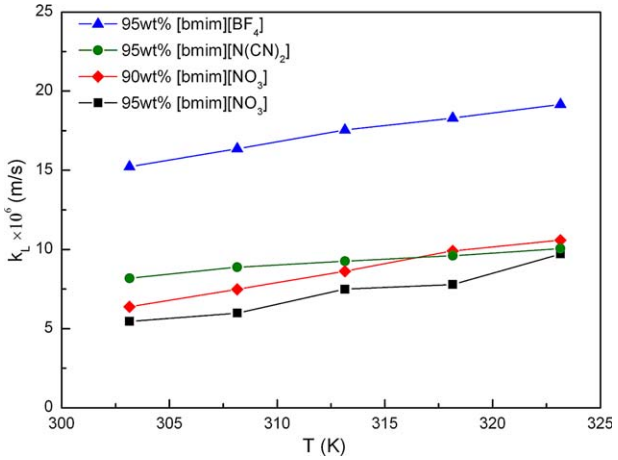

Figure 8. k_L in different IL-H_2O systems over the temperature range from 303 to 323 K.

[Color figure can be viewed in the online issue, which is available at wileyonlinelibrary.com.]

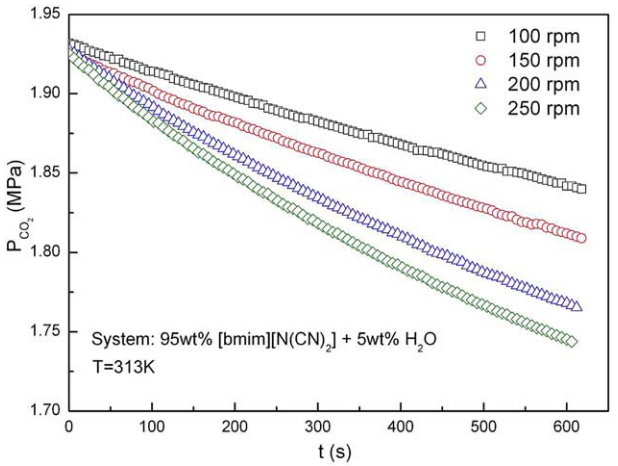

Figure 9. Effect of stirrer speed on the pressure drop in IL-H2O system.

[Color figure can be viewed in the online issue, which is available at wileyonlinelibrary.com.]

anions. The diffusion coefficient of CO_2 increases with the increase of CO_2 concentration[43,44] and the viscosity reduction effect of ILs after absorbing CO_2 depends on the different structures of ILs. Therefore, it is reasonable to deduce that k_L in IL is also influenced by the structures of ILs. When comparing [bmim][BF_4] with [omim][BF_4], in view of the cationic impact on the CO_2 solubility the fact that k_L in [omim][BF_4] is greater can be explained.

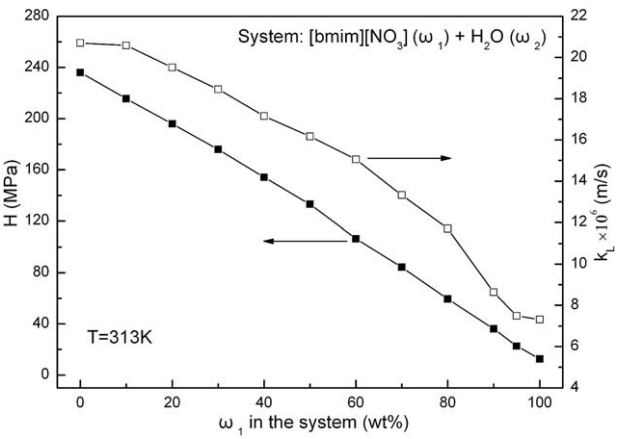

Figure 10. Effect of IL concentration on the Henry's constant and k_L in IL-H_2O system.

Table 5. Available k_L Values of Absorbing CO_2 in Water and in IL

Temperature (K)	Solvent	$k_L \times 10^5$ (m s^{-1})	Reference
303	Water	4.19	Lu et al.[32]
303	Water	1.6	Konduru et al.[45]
298–328	Water	7.1–13.6	Qin et al.[46]
313	Water	2.8	Bishnoi et al.[47]
303	[bmim][BF_4]	0.75–1.39	Sanchez et al.[30]
313	[bmim][BF_4]	1.28	This work
303	95 wt % bmim[BF_4] + 5 wt % H_2O	1.52	This work
303	95 wt % bmim[NO_3] +5 wt % H_2O	0.55	This work
303	90 wt % bmim[NO_3] + 5 wt % H_2O	0.64	This work

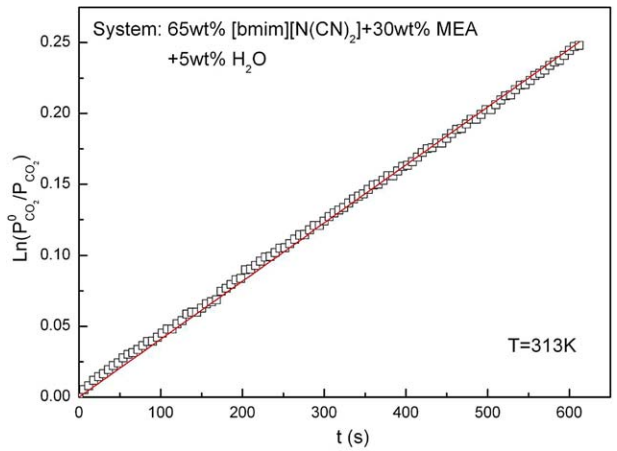

Figure 11. Enhancement factor determination in MEA-IL-H2O system.

[Color figure can be viewed in the online issue, which is available at wileyonlinelibrary.com.]

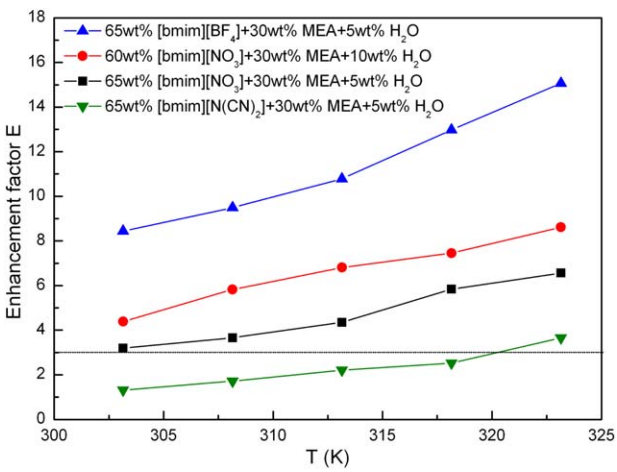

Figure 12. Enhancement factors in different MEA-IL-H_2O systems from 303 to 323 K.

[Color figure can be viewed in the online issue, which is available at wileyonlinelibrary.com.]

Table 6. Kinetic Parameters of MEA-[bmim][NO_3]-H_2O Systems at 313 K

Composition of the Absorbent										
IL	H_2O	MEA (wt %)	C_{MEA} (mol·m^{-3})	$D_{CO_2}\times10^{10}$ (m^2·s^{-1})	$D_{MEA_2}\times10^{10}$ (m^2 s^{-1})	$k_L\times10^6$ (m·s^{-1})	k_2 (L·mol^{-1} s^{-1})	k_{ps} (s^{-1})	*Ha*	E_i
70 wt % [bmim][NO_3]	0	30	5403.86	6.23	0.11	7.31	0.08	0.45	2.29	11.62
65 wt % [bmim][NO_3]	5	30	5384.78	7.44	0.91	7.5	0.27	1.43	4.36	88.20
60 wt % [bmim][NO_3]	10	30	5367.48	8.12	1.71	8.63	0.79	4.25	6.81	180.87
50 wt % [bmim][NO_3]	20	30	5289.36	10.1	2.97	11.71	2.53	13.35	9.92	273.38
40 wt % [bmim][NO_3]	30	30	5222.85	11.98	4.24	13.32	3.92	20.47	11.75	350.38
30 wt % [bmim][NO_3]	40	30	5150.14	13.88	5.44	15.06	7.01	36.06	14.86	391.74
20 wt % [bmim][NO_3]	50	30	5077.46	15.72	6.26	16.17	15.99	81.18	22.09	415.36
10 wt % [bmim][NO_3]	60	30	5002.44	17.53	8.73	17.16	24.72	123.67	27.14	514.49
0	70	30	4928.4	19.18	18.27	18.46	57.26	282.19	39.86	988.53

As depicted in Figure 6, the k_L determination in different IL-H_2O systems was investigated at 313 K. These three IL-H_2O systems, namely 95 wt % [bmim][BF_4], 95 wt % [bmim][$N(CN)_2$], and 90 wt % [bmim][NO_3] have very similar viscosities (13.87, 11.27, and 12.65 mPa s, respectively) and show different slopes for calculating k_L, which can be mainly attributed to the effect of IL structure on the CO_2 solubility in these IL-H_2O systems. Comparing the 95 wt % [bmim][NO_3] system with the 90 wt % [bmim][NO_3] system, the different values of the slopes lie in the difference of viscosity. Therefore, as expected, k_L in IL-H_2O systems depends on both the viscosity and the structure of ILs.

Effect of Temperature. As presented in Figure 7, the effect of temperature on k_L determination was investigated over the temperature range from 303 to 323 K. It shows that the slopes increase with the increase of system temperature. Detailed data of k_L in different IL-H_2O systems has been displayed in Figure 8. The k_L in 95 wt % [bmim][BF_4] system is much larger than that in other three IL-H_2O systems, which can be ascribed to the influence of IL structure. The temperature has a positive influence on the diffusivity of CO_2 in the IL-H_2O systems due to the decrease of viscosity, which is beneficial for increasing the CO_2 mass-transfer coefficients.

Effect of Stirrer Speed. As typically shown in Figure 9, the influence of the stirrer speed was investigated by detecting the speed of pressure drop in the IL-H_2O system. In the present study, the stirrer speed is limited to 250 rpm to ensure an undisturbed interface. It is found that a higher stirrer speed can result in a higher speed of pressure drop in the reactor, which can be attributed to a greater k_L.

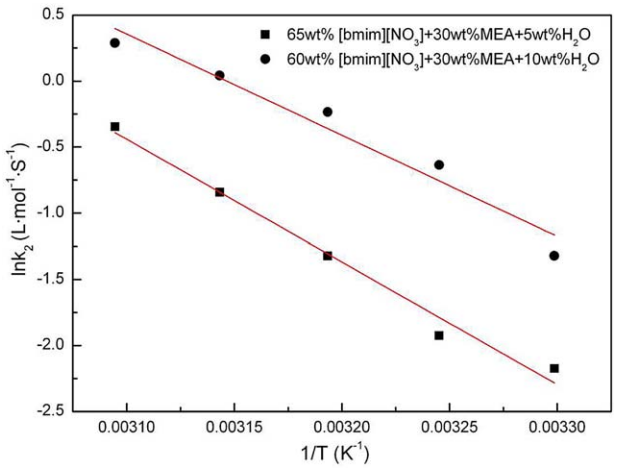

Figure 13. Activation energy determination in MEA-[bmim][NO3]-H_2O systems.

[Color figure can be viewed in the online issue, which is available at wileyonlinelibrary.com.]

Effect of IL Concentration. The ratio of IL to H_2O in the absorbent, which is an important parameter for CO_2 absorption process, was studied over a wide range of IL concentrations from 0 to 100 wt %. Figure 10 shows that the Henry's constant decreases, namely the CO_2 solubility increases with continuously adding IL [bmim][NO_3] into the system. However, from the viewpoint of mass transfer, the k_L decreases with the increase of IL concentrations which can be ascribed to the increase of viscosity. Therefore, when determining the suitable ratio of IL to H_2O in the absorbent for CO_2 physical absorption, both the thermodynamic and dynamic factors should be taken into consideration.

Kinetic parameters

Enhancement Factor. The enhancement factor was calculated by Eq. 12. The liquid-side mass-transfer coefficient obtained in the IL-H_2O systems was applied to determine E in the MEA-IL-H_2O systems. Similar approximation has been reported in different research groups,[32,45–47] who used water as liquid phase to determine k_L in studying the kinetics of CO_2 chemical absorption into different amine aqueous systems. The available k_L values of absorbing CO_2 in water and in IL have been presented in Table 5. It shows that the mass-transfer process of absorbing CO_2 is faster in water than in IL, which can be attributed to the higher viscosity of IL. Adding water to IL can decrease the viscosity, which will speed up the mass-transfer process.

A typical plot for enhancement factor determination in the MEA-IL-H_2O system at 313 K has been presented in Figure 11. It shows an excellent linear trend, which ensure the accuracy of the method used in the present study to calculate E. The values of experimental enhancement factors in different MEA-IL-H_2O systems are shown in Figure 12. The enhancement factors increase with the increase of temperature. The enhancement factor nearly doubles at 323 K compared with that at 303 K. Figure 12 also displays that the enhancement factors are ranked as 65 wt% [bmim][$N(CN)_2$] < 65 wt% [bmim][NO_3] < 60 wt% [bmim][NO_3] < 65 wt% [bmim][BF_4]. Interestingly, when adding [bmim][$N(CN)_2$] into MEA aqueous system, the enhancement factors are mostly below 3, indicating that the reaction regime has changed from fast regime ($E = Ha$) to intermediate between slow ($E = 1$) and fast regime. However, for other MEA-IL-H_2O systems, the reaction regime keeps in the fast regime. Therefore, in view of the dynamics, the IL [bmim][$N(CN)_2$] is not suitable to be added into the MEA aqueous system.

Table 7. Available E_a Values of the Reaction Between CO_2 and MEA in the Literature

Temperature (K)	MEA Concentration	Reactor	E_a (kJ·mol^{-1})	Reference
298–323	0.5–12 mol L^{-1}	Stirred cell reactor	44.88	Ying et al.[2]
293–333	3–9 mol L^{-1}	Laminar jet	36.68	Aboudheir et al.[49]
303–313	0.1–0.5 mol L^{-1}	Wetted wall column	51.9	Liao et al.[50]
298–333	3,5, 7 wt %	Laminar jet	31.61	Ramachandran et al.[51]

Moreover, it has been reported that the anion $[BF_4]^-$ will generate the very toxic and corrosive substance HF when the system contains water for a long time.[33] And the reaction to produce HF from $[BF_4]^-$ will be accelerated during the CO_2 desorption process because the desorption temperature is usually high (about 100°C). Therefore, in view of both the mass-transfer rates and the stability of IL in CO_2 absorption system, the new system MEA + [bmim][NO_3] + H_2O is recommended and will be studied further in the next part.

Reaction Rate Constant. It is safe to ignore the chemical reaction between the ILs choosen in the present study and CO_2. The pseudofirst-order reaction rate constant is given by

$$k_{ps} = k_2 C_{MEA} \tag{31}$$

The k_{ps} was studied in the MEA-[bmim][NO_3]-H_2O system over a wide range of IL concentrations from 0 to 70 wt%. According to the literature,[48] the reaction rate of CO_2 in water is very slow ($k = 0.026$ s^{-1} at 298 K), which is much slower than the reaction in MEA-[bmim][NO_3]-H_2O system. This can be ascribed to the fact that the MEA-[bmim][NO_3]-H_2O system has a stronger alkalinity (pH = 12.58 at 298 K) than water. Due to the negligible contribution, the reaction of CO_2 with water can be neglected. The detailed kinetic parameters in MEA-[bmim][NO_3]-H_2O systems at 313 K has been displayed in Table 6. It clearly shows that the calculated Hatta number and infinite enhancement factor satisfy the criterion of Eq. 13, ensuring the validation of the fast pseudofirst-order reaction regime in this work. According to Table 6, D_{MEA} changes stronger than k_L andD_{CO_2}. It has been illustrated in the previous description that k_L in IL systems is influenced not only by the viscosity but also the molecular structures of ILs. Therefore, the viscosity has a stronger impact on D_{MEA} than k_L, which results in the greater change of D_{MEA}. As for the comparison of D_{MEA} and D_{CO_2}, it can be referred to Eqs. 17–21. It displays that D_{MEA} andD_{CO_2} are inversely proportional to $\mu_{IL\text{-}H_2O}$ and $\mu^{0.51}$, respectively. The values of $\mu_{IL\text{-}H_2O}$ and μ are very close. Therefore, the greater change of D_{MEA} can be attributed to the fact that the viscosity exerts a stronger influence on D_{MEA}. Moreover, D_{MEA}, D_{CO_2} and k_L increase with decreasing the IL concentrations in the systems, which strengthen the reaction rates.

Activation Energy. The calculated values of kinetic parameter k_2 were applied to determine the activation energy (E_a) using the Arrhenius equation. A typical Arrhenius plot for calculating activation energy in MEA-[bmim][NO_3]-H_2O systems from 303 to 323 K has been depicted in Figure 13. The values in Figure 13 have been correlated to calculate the activation energy as follows:

absorbent: 30 wt % MEA + 65 wt % [bmim][NO_3] + 5 wt % H_2O

$$\ln k_2 = \frac{-9275}{T} + 28.311 \tag{32}$$

absorbent: 30 wt % MEA + 60 wt % [bmim][NO_3] + 10 wt % H_2O

$$\ln k_2 = \frac{-7661}{T} + 24.105 \tag{33}$$

The values of the activation energy are 77.11 and 63.69 kJ mol^{-1} for the two MEA-[bmim][NO_3]-H_2O systems, respectively. The obtained results have been compared with the available E_a values of the reaction between CO_2 and MEA aqueous systems reported in different literature,[2,49–51] which has been listed in Table 7. It demonstrates that E_a increases when adding IL into the MEA aqueous system to absorb CO_2. In addition, the E_a decreases with the decrease of IL concentration in the MEA-[bmim][NO_3]-H_2O system.

Conclusions

Mixing ILs with amine is considered as a promising way to make ILs being directly applicable in a carbon capture system. The lack of mass-transfer study, especially the liquid-side mass-transfer coefficient, has become a bottleneck in developing such novel CO_2 capture process. In this work, the liquid-side mass-transfer coefficient was determined by the decreasing pressure method in a stirred cell reactor with an undisturbed gas–liquid interface at temperatures ranging from 303 to 323 K. The kinetics of chemical absorption of CO_2 with aqueous mixed solvents was studied in ILs-based systems containing 30 wt % MEA and 0–70 wt % ILs.

The results demonstrate that k_L is influenced both by the viscosity and the molecular structure of ILs. The k_L decreases while CO_2 solubility increases with the increase of IL concentrations. The kinetics of the reaction between CO_2 and different MEA-IL-H_2O systems were studied over a wide range of IL concentrations from 0 to 70 wt %. The [bmim][$N(CN)_2$] IL is not suitable to be added into the aqueous MEA system because of greatly slowing the reaction rates. The new system MEA + [bmim][NO_3] + H_2O is recommended as a promising candidate for CO_2 absorption. The overall reaction rates increase with decreasing the IL concentrations in the MEA-[bmim][NO_3]-H_2O systems. The E_a values of the reaction of CO_2 absorption with the MEA-[bmim][NO_3]-H_2O systems are greater but the same order of magnitude as the available E_a data in the literature using MEA aqueous system.

Acknowledgments

The authors acknowledge gratefully for the financial supports from the National Basic Research Program of China (973 Program) (2013CB733506, 2014CB744306), the Key Program of National Natural Science Foundation of China (No.21036007) and the National Natural Science Foundation

of China (No.51274183). This contribution was identified by Kriston P Brooks (Pacific Northwest National Laboratory) as the best presentation in the session "Unconventional Technologies for CO_2 Capture, Conversion and Utilization I" of the 2012 AIChE Annual Meeting in Pittsburgh, PA.

Notation

List of symbols

a = specific gas-liquid interfacial area, $m^2\ m^{-3}$
A = gas–liquid interfacial area, m^2
C = concentration, mol m^{-3}
D = diffusivity, $m^2\ s^{-1}$
E = enhancement factor
E_a = activation energy, kJ mol^{-1}
E_∞ = infinite enhancement factor
f = fugacity, kPa
H = Henry's constant, kPa
Ha = Hatta number
k_1 = reaction rate constant with respect to CO_2, $m^3\ mol^{-1}\ s^{-1}$
k_2 = second-order reaction rate constant, $m^3\ mol^{-1}\ s^{-1}$
K_H = Henry's constant, Pa $m^3\ mol^{-1}$
k_L = liquid-side mass-transfer coefficient, m s^{-1}
k_{ps} = pseudofirst-order reaction rate constant, s^{-1}
M = molecular weight, g mol^{-1}
n = mole amount, mol
N = overall mass-transfer flux, mol s^{-1}
P = pressure, kPa
P_c = critical pressure, kPa
P^e = equilibrium pressure, kPa
P^0 = initial pressure, kPa
P_{Vapor} = vapour pressure, kPa
r = reaction rate, $m^3\ mol^{-1}\ s^{-1}$
R = gas constant, J $K^{-1}\ mol^{-1}$
t = time, s
T = temperature, K
T_c = critical temperature, K
V = volume, cm^3
x = mole fraction
Z = compressibility factor

Abbreviations

EOS = equation of state
IL = ionic liquid
MEA = monoethanolamine
TSIL = task-specific ionic liquid

Greek letters

ρ = density, $g{\cdot}cm^{-3}$
μ = viscosity, mPa s
φ = fugacity coefficient
v = stoichiometric coefficient
β = parameter
ω = mass fraction, wt %

Subscripts

G = gas phase
L = liquid phase

Literature Cited

1. Camacho F, Sanchez S, Pacheco R, Sanchez A, La Rubia M. Thermal effects of CO_2 absorption in aqueous solutions of 2-amino-2-methyl-1-propanol. *AIChE J*. 2005;51:2769–2777.
2. Ying J, Eimer DA. Determination and measurements of mass transfer kinetics of CO_2 in concentrated aqueous monoethanolamine solutions by a stirred cell. *Ind Eng Chem Res*. 2013;52:2548–2559.
3. García-Abuín A, Gómez-Díaz D, Navaza JM, Vidal-Tato I. Kinetics of carbon dioxide chemical absorption into cyclic amines solutions. *AIChE J*. 2011;57:2244–2250.
4. Gómez-Díaz D, Navaza JM. Kinetics of carbon dioxide absorption into aqueous glucosamine solutions. *AIChE J*. 2008;54:321–326.
5. Huang Y, Dong HF, Zhang XP, Li CS, Zhang SJ. A new fragment contribution-corresponding states method for physicochemical properties prediction of ionic liquids. *AIChE J*. 2013;59:1348–1359.
6. Zhang X, Liu Z, Wang W. Screening of ionic liquids to capture CO_2 by COSMO-RS and experiments. *AIChE J*. 2008;54:2717–2728.
7. Ficke LE, Brennecke JF. Interactions of ionic liquids and water. *J Phys Chem B*. 2010;114:10496–10501.
8. Blanchard LA, Hancu D, Beckman EJ, Brennecke JF. Green processing using ionic liquids and CO_2. *Nature*. 1999;399:28–29.
9. Chen Y, Zhang S, Yuan X, Zhang Y, Zhang X, Dai W, Mori R. Solubility of CO_2 in imidazolium-based tetrafluoroborate ionic liquids. *Thermochim Acta*. 2006;441:42–44.
10. Bates ED, Mayton RD, Ntai I, Davis JH. CO_2 capture by a task-specific ionic liquid. *J Am Chem Soc*. 2002;124:926–927.
11. Zhang J, Zhang S, Dong K, Zhang Y, Shen Y, Lv X. Supported absorption of CO_2 by tetrabutylphosphonium amino acid ionic liquids. *Chem Eur J*. 2006;12:4021–4026.
12. Gurkan BE, de la Fuente JC, Mindrup EM, Ficke LE, Goodrich BF, Price EA, Schneider WF, Brennecke JF. Equimolar CO_2 absorption by anion-functionalized ionic liquids. *J Am Chem Soc*. 2010;132:2116–2117.
13. Zhang Y, Zhang S, Lu X, Zhou Q, Fan W, Zhang X. Dual amino-functionalised phosphonium ionic liquids for CO_2 capture. *Chem Eur J*. 2009;15:3003–3011.
14. Zhang J, Jia C, Dong H, Wang J, Zhang X, Zhang S. A novel dual amino-functionalized cation-tethered ionic liquid for CO_2 capture. *Ind Eng Chem Res*. 2013;52:5835–5841.
15. Camper D, Bara JE, Gin DL, Noble RD. Room-temperature ionic liquid-amine solutions: Tunable solvents for efficient and reversible capture of CO_2. *Ind Eng Chem Res*. 2008;47:8496–8498.
16. Ahmady A, Hashim MA, Aroua MK. Absorption of carbon dioxide in the aqueous mixtures of methyldiethanolamine with three types of imidazolium-based ionic liquids. *Fluid Phase Equilib*. 2011;309:76–82.
17. Zhang F, Fang C, Wu Y, Wang Y, Li A, Zhang Z. Absorption of CO_2 in the aqueous solutions of functionalized ionic liquids and MDEA. *Chem Eng J*. 2010;160:691–697.
18. Ahmady A, Hashim MA, Aroua MK. Density, viscosity, physical solubility and diffusivity of CO_2 in aqueous MDEA+ [bmim][BF_4] solutions from 303 to 333K. *Chem Eng J*. 2011;172:763–770.
19. Zhao Y, Zhang X, Zeng S, Zhou Q, Dong H, Tian X, Zhang S. Density, viscosity, and performances of carbon dioxide capture in 16 absorbents of amine+ ionic liquid+ H_2O, ionic liquid+ H_2O, and amine+ H_2O systems. *J Chem Eng Data*. 2010;55:3513–3519.
20. Tagawa A, Dohi N, Kawase Y. Volumetric gas-liquid mass transfer coefficient in aerated stirred tank reactors with dense floating solid particles. *Ind Eng Chem Res*. 2012;51:1938–1948.
21. Poncin S, Nguyen C, Midoux N, Breysse J. Hydrodynamics and volumetric gas-liquid mass transfer coefficient of a stirred vessel equipped with a gas-inducing impeller. *Chem Eng Sci*. 2002;57:3299–3306.
22. Alves SS, Maia CI, Vasconcelos JMT. Gas-liquid mass transfer coefficient in stirred tanks interpreted through bubble contamination kinetics. *Chem Eng Process*. 2004;43:823–830.
23. Martin M, Montes F, Galan MA. Mass transfer rates from bubbles in stirred tanks operating with viscous fluids. *Chem Eng Sci*. 2010;65:3814–3824.
24. Dong HF, Wang XL, Liu L, Zhang XP, Zhang SJ. The rise and deformation of a single bubble in ionic liquids. *Chem Eng Sci*. 2010;65:3240–3248.
25. Wang XL, Dong HF, Zhang XP, Xu Y, Zhang SJ. Numerical simulation of absorbing CO_2 with ionic liquids. *Chem Eng Technol*. 2010;33:1615–1624.
26. Wang XL, Dong HF, Zhang XP, Yu L, Zhang SJ, Xu Y. Numerical simulation of single bubble motion in ionic liquids. *Chem Eng Sci*. 2010;65:6036–6047.
27. Zhang X, Dong HF, Huang Y, Li CS, Zhang XP. Experimental study on gas holdup and bubble behavior in carbon capture systems with ionic liquid. *Chem Eng J*. 2012;209:607–615.
28. Zhang X, Dong H, Bao D, Huang Y, Zhang X, Zhang S. Effect of small amount of water on CO_2 bubble behavior in ionic liquid systems. *Ind Eng Chem Res*. 2014;53:428–439.

29. Zhang L, Wang J, Xiang Y, Zeng X, Chen J. Absorption of carbon dioxide with ionic liquid in a rotating packed bed contactor: Mass transfer study. *Ind Eng. Chem Res.* 2011;50:6957–6964.
30. Sanchez LMG, Meindersma GW, de Haan AB. Kinetics of absorption of CO_2 in amino-functionalized ionic liquids. *Chem Eng J.* 2011;166:1104–1115.
31. Ahmady A, Hashim MA, Aroua MK. Kinetics of carbon dioxide absorption into aqueous MDEA + [bmim][BF_4] solutions from 303 to 333 K. *Chem Eng J.* 2012;200:317–328.
32. Lu BH, Wang XQ, Xia YF, Liu N, Li SJ, Li W. Kinetics of carbon dioxide absorption into mixed aqueous solutions of MEA + Bmim[BF_4] using a double stirred cell. *Energy Fuels.* 2013;27:6002–6009.
33. Villagran C, Deetlefs M, Pitner WR, Hardacre C. Quantification of halide in ionic liquids using ion chromatography. *Anal Chem.* 2004; 76:2118–2123.
34. Caplow M. Kinetics of carbamate formation and breakdown. *J Am Chem Soc.* 1968;90:6795–6803.
35. Danckwerts P. The reaction of CO_2 with ethanolamines. *Chem Eng Sci.* 1979;34:443–446.
36. Versteeg GF, Van Swaalj W. Solubility and diffusivity of acid gases (carbon dioxide, nitrous oxide) in aqueous alkanolamine solutions. *J Chem Eng Data.* 1988;33:29–34.
37. Sada E, Kumazawa H, Butt M. Solubility and diffusivity of gases in aqueous solutions of amines. *J Chem Eng Data.* 1978;23: 161–163.
38. Wilke C, Chang P. Correlation of diffusion coefficients in dilute solutions. *AIChE J.* 1955;1:264–270.
39. Aki SN, Mellein BR, Saurer EM, Brennecke JF. High-pressure phase behavior of carbon dioxide with imidazolium-based ionic liquids. *J Phys Chem B.* 2004;108:20355–20365.
40. Costa Gomes M. Low-pressure solubility and thermodynamics of solvation of carbon dioxide, ethane, and hydrogen in 1-hexyl-3-methylimidazolium bis (trifluoromethylsulfonyl) amide between temperatures of 283 K and 343 K. *J Chem Eng Data.* 2007;52: 472–475.
41. Redlich O, Kwong J. On the thermodynamics of solutions. V. An equation of state fugacities of gaseous solutions. *Chem Rev.* 1949; 44:233–244.
42. Zhang XP, Zhang XC, Dong HF, Zhao ZJ, Zhang SJ, Huang Y. Carbon capture with ionic liquids: overview and progress. *Energy Environ Sci.* 2012;5:6668–6681.
43. Bhargava B, Krishna A, Balasubramanian S. Molecular dynamics simulation studies of CO_2–[bmim][PF_6] solutions: Effect of CO_2 concentration. *AIChE J.* 2008;54:2971–2978.
44. Zhang X, Liu X, Yao X, Zhang S. Microscopic structure, interaction and properties of a guanidinium-based ionic liquid and its mixture with CO_2. *Ind Eng Chem Res.* 2011;50:8323–8332.
45. Konduru PB, Vaidya PD, Kenig EY. Kinetics of removal of carbon dioxide by aqueous solutions of N,N-diethylethanolamine and piperazine. *Environ Sci Technol.* 2010;44:2138–2143.
46. Qin F, Wang S, Hartono A, Svendsen HF, Chen C. Kinetics of CO_2 absorption in aqueous ammonia solution. *Int J Greenh Gas Control.* 2010;4:729–738.
47. Bishnoi S, Rochelle GT. Absorption of carbon dioxide in aqueous piperazine/methyldiethanolamine. *AIChE J.* 2002;48:2788–2799.
48. Ko JJ, Li MH. Kinetics of absorption of carbon dioxide into solutions of N-methyldiethanolamine + water. *Chem Eng Sci.* 2000;55: 4139–4147.
49. Aboudheir A, Tontiwachwuthikul P, Chakma A, Idem R. Kinetics of the reactive absorption of carbon dioxide in high CO_2-loaded, concentrated aqueous monoethanolamine solutions. *Chem Eng Sci.* 2003;58:5195–5210.
50. Liao CH, Li MH. Kinetics of absorption of carbon dioxide into aqueous solutions of monoethanolamine plus N-methyldiethanolamine. *Chem Eng Sci.* 2002;57:4569–4582.
51. Ramachandran N, Aboudheir A, Idem R, Tontiwachwuthikul P. Kinetics of the absorption of CO_2 into mixed aqueous loaded solutions of monoethanolamine and methyldiethanolamine. *Ind Eng Chem Res.* 2006;45:2608–2616.

Manuscript received Jan. 21, 2014, and revision received Apr. 15, 2014.